Design of a Robust Component-wise Sliding Mode Controller for a Two-Link Manipulator

Mohammed Qasim [1*], Abdulla Ibrahim Abdulla [2], Abdurahman Basil Ayoub [3]
[1, 2, 3,] Department of Systems and Control Engineering, Ninevah University, Mosul, Iraq
Email: [1] mohammed.qasim@uoninevah.edu.iq, [2] abdullah.abdullah@uoninevah.edu.iq,
[3] abdulrahman.ayoub@uoninevah.edu.iq
*Corresponding Author

***Abstract*—Compared to conventional Multiple-Input Multiple-Output (MIMO) Sliding Mode Control (SMC) techniques, the component-wise SMC approach offers several advantages, including improved decoupling of system dynamics, enhanced robustness, and greater flexibility in controller design. This paper proposes a novel trajectory tracking controller for a two-link manipulator based on the component-wise sliding mode control approach. The design methodology involves determining controller gains by solving a set of inequalities. This analysis results in conditions on the system parameter uncertainties that guarantee the existence of a feasible solution to the set of inequalities. Furthermore, an algorithm is presented to determine the maximum allowable uncertainties that ensure the feasibility of the controller gains. To evaluate the performance and robustness of the proposed tracking controller, the manipulator is subjected to a series of challenging trajectories, including circular and figure-8 ones, under both nominal and maximum allowable uncertainty conditions. The proposed controller demonstrates superior performance across both circular and figure-8 trajectories, exhibiting excellent transient response and minimal steady-state error even under the maximum permissible uncertainties, which extend up to 27% in link masses. This performance is validated through a quantitative analysis that incorporates a comparative evaluation against two conventional MIMO SMC techniques. The comparison is conducted using the Integral Norm of Error (INE) to assess tracking accuracy and the Integral Norm of Control Action (INU) to evaluate the energy efficiency of the controllers. These metrics provide a comprehensive basis for analyzing both the precision and the energy consumption of the proposed control strategy in relation to established methods.**

Keywords—*Two-Link Manipulator; Sliding Mode Control; Style; Component-Wise SMC; Model Uncertainties.*

I. INTRODUCTION

Robotics are becoming crucial in many industrial, academic, and real-world applications [1]-[5]. The basic requirements for manipulators control are rapid transient response and precise tracking performance [6]-[9]. The design of a robust controller with the required performance for a robot manipulator is still a noteworthy challenge since the robotic manipulator is typically a highly nonlinear system with a coupled MIMO that can be affected by disturbances and uncertainties in real-life [10]-[13]. These disturbances, including joint friction, payload change, and external forces, can lead to instability and influence system performance [14]-[16].

Many control schemes, including fuzzy control [17]-[19], optimal control [20], adaptive control [21]-[24], vision-based control [25]-[27], PID control [28]-[30], shared control [31]-[33], artificial neural network control [34]-[36], predictive control [37]-[41], feedback linearization based control [42]-[44], and sliding mode control [45]-[50], have been proposed in recent years in existing research to achieve acceptable control performance of robotics and manipulators. SMC has attracted extensive research attention in controlling robotic manipulators due to its robustness to external disturbances and uncertainties, and fast transient response [51]-[52]. However, conventional MIMO SMC approaches tend to employ a global sliding surface, which may not adequately exploit the unique dynamics of multi-link robotic manipulators [53]-[55]. Conventional MIMO SMC approaches often simplify the design process by disregarding system dynamics that are assumed to have negligible effects. However, this simplification can result in the under- or over-estimation of controller gains, which compromises the robustness of the system. The implementation of MIMO SMC approaches in real-life applications can be impacted by its complex tuning and design methods. In addition, it is required to design an efficient SMC that handles singularities, chattering phenomena, and sluggish convergence while handling the trajectory tracking problem of the manipulator.

To address the problems discussed above, an approach of controlling each manipulator joint alone, called component-wise SMC, can be used [56]-[58]. This approach can simplify the control design and can improve the response time and accuracy of robotic manipulators, especially when the dynamic variations are critical. Practical implementation of this approach poses challenges, particularly in determining appropriate gains for each SMC channel. Solving the associated set of inequalities may not always yield feasible solutions for the controller gains [59].

This work presents a novel component-wise SMC approach for trajectory tracking of a two-link manipulator while addressing the aforementioned challenges. The proposed approach simplifies the controller design procedure to ensure a feasible solution for the SMC gain. Furthermore, this work aims to design and validate a control approach that maintains the desired performance even when there are large uncertainties related to link masses. Two different trajectories, circular and figure-8, are utilized in this paper for the MATLAB-based simulations to evaluate the performance of the proposed component-wise SMC with link masses uncertainties of 27%. Finally, to demonstrate the superiority of the proposed control approach, the simulation results are assessed in relation to conventional component-wise/MIMO SMC approaches.

This paper's main contribution can be summed up as follows:

- Establishing a rigorous and systematic framework for component-wise SMC design and
- Developing a methodology for quantifying the maximum permissible uncertainties in system dynamics under the proposed component-wise SMC.

The arrangement of this paper is as follows. In Section 2, the modeling of the planer two-link manipulator is provided. The proposed sliding mode controller for manipulator control is presented in Section 3. Results and discussions are given in Section 4. The paper's conclusion is found in Section 5.

II. Two-link Manipulator Modeling

A planar manipulator with two revolute joints is considered in this study. Fig. 1 illustrates the manipulator along with its associated variables.

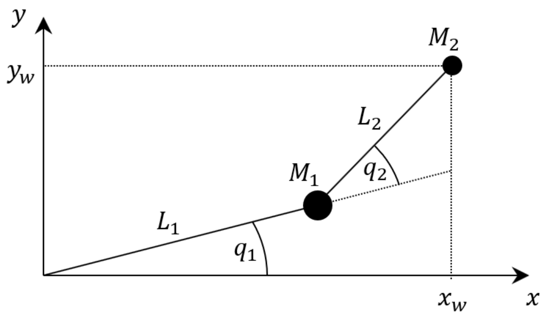

Fig. 1. Two-link manipulator configuration: showing link lengths and masses and joint displacements

A geometric analysis of Fig. 1 facilitates the derivation of the forward kinematics for the two-link manipulator. The end-effector position, denoted by (x_w, y_w) and coinciding with the location of mass M_2 in the world coordinate frame (x, y), is given by

$$\begin{aligned} x_w &= L_1 \cos q_1 + L_2 \cos(q_1 + q_2) \\ y_w &= L_1 \sin q_1 + L_2 \sin(q_1 + q_2) \end{aligned} \tag{1}$$

where q_1 and q_2 represent the joint displacements, while L_1 and L_2 denote the links' lengths. By solving (1) for the joint displacements with respect to the end-effector position (x_w, y_w), the inverse kinematics is determined as follows

$$\begin{aligned} q_2 &= atan2(D, C) \\ q_1 &= -atan2(L_2 sin q_2, L_1 + L_2 cos q_2) \\ &\quad + atan2(y_w, x_w) \end{aligned} \tag{2}$$

where $C = \frac{x_w^2 + y_w^2 - L_1^2 - L_2^2}{2L_1L_2}$ and $D = \pm\sqrt{1 - C^2}$. The non-uniqueness of this solution arises from the dual sign possibilities inherent in the square root operation applied to variable D. The function atan2(.) represents a four-quadrant inverse tangent that returns values in the closed interval $[-\pi, \pi]$.

Utilizing a common modeling approach, such as the Euler-Lagrange equations, results in the dynamic model, described by [60].

$$\begin{bmatrix} \tau_1 \\ \tau_2 \end{bmatrix} = \begin{bmatrix} m_{11} & m_{12} \\ m_{12} & m_{22} \end{bmatrix} \begin{bmatrix} \ddot{q}_1 \\ \ddot{q}_2 \end{bmatrix} + \begin{bmatrix} n_1 \\ n_2 \end{bmatrix} \tag{3}$$

with

$$\begin{aligned} m_{11} &= L_1^2(M_1 + M_2) + L_2^2 M_2 + 2L_1L_2M_2 \cos q_2 \\ m_{12} &= L_2^2 M_2 + L_1 L_2 M_2 \cos q_2 \\ m_{22} &= L_2^2 M_2 \\ \boldsymbol{M(q)} &= \begin{bmatrix} m_{11} & m_{12} \\ m_{21} & m_{22} \end{bmatrix} \\ n_1 &= -L_1L_2M_2(2\dot{q}_1\dot{q}_2 - \dot{q}_2^2) sin q_2 \\ n_2 &= L_1L_2M_2\dot{q}_1^2 sin q_2 \\ \boldsymbol{N(q, \dot{q})} &= \begin{bmatrix} n_1 \\ n_2 \end{bmatrix} \end{aligned} \tag{4}$$

Observe that (4) lacks gravity terms since the manipulator operates in a plane perpendicular to gravity. Henceforth, the dependency of $\boldsymbol{M(q)}$ and $\boldsymbol{N(q, \dot{q})}$ on $\boldsymbol{q} = [q_1\ q_2]^T$ and $\dot{\boldsymbol{q}} = [\dot{q}_1\ \dot{q}_2]^T$ will be omitted for simplicity.

III. Proposed Sliding Mode Controller

By introducing the state variables $\boldsymbol{z}_1 = \boldsymbol{q}, \boldsymbol{z}_2 = \dot{\boldsymbol{q}}$ and defining the input vector $\boldsymbol{u} = [\tau_1\ \tau_2]^T$, the system in (3) is recast in standard regular form

$$\begin{aligned} \dot{\boldsymbol{z}}_1 &= \boldsymbol{z}_2 \\ \dot{\boldsymbol{z}}_2 &= \boldsymbol{M}^{-1}(\boldsymbol{u} - \boldsymbol{N}) \end{aligned} \tag{5}$$

Certain link lengths are assumed, meaning that the uncertainties are only in M_1 and M_2. These can be represented as

$$\begin{aligned} M_1 &= \widetilde{M}_1 + \delta_{m1}, \qquad |\delta_{m1}| < c_1\widetilde{M}_1 \\ M_2 &= \widetilde{M}_2 + \delta_{m2}, \qquad |\delta_{m2}| < c_2\widetilde{M}_2 \end{aligned} \tag{6}$$

where $\widetilde{M}_i$ and δ_{mi} denote the nominal and perturbation values of M_i and δ_{mi} respectively with $i = 1,2$ while $c_i \in \boldsymbol{\mathcal{R}}_+$ is a positive constant, to be determined later.

Thus, the matrix $\boldsymbol{N}$ can be expressed as a nominal and perturbation term as

$$\boldsymbol{N} = (\boldsymbol{N_o} + \boldsymbol{\delta_N}) \tag{7}$$

where

$$\begin{aligned} \boldsymbol{N_o} &= \begin{bmatrix} -L_1L_2\widetilde{M}_2(2\dot{q}_1\dot{q}_2 - \dot{q}_2^2) sin q_2 \\ L_1L_2\widetilde{M}_2 x_3^2 \sin x_2 \end{bmatrix} \\ \boldsymbol{\delta_N} &= \begin{bmatrix} -L_1L_2\delta_{m2}(2\dot{q}_1\dot{q}_2 - \dot{q}_2^2) sin q_2 \\ L_1L_2\delta_{m2} x_3^2 \sin x_2 \end{bmatrix} \end{aligned} \tag{8}$$

Assume that the control action is defined by $\boldsymbol{u} = \boldsymbol{u_0} + \boldsymbol{u_s}$ and let $\boldsymbol{u_0} = \boldsymbol{N_0}$, consequently, (5) transforms into

$$\begin{aligned}\dot{\boldsymbol{z}}_1 &= \boldsymbol{z}_2\\ \dot{\boldsymbol{z}}_2 &= \boldsymbol{M}^{-1}(\boldsymbol{u}_s - \boldsymbol{\delta}_N)\end{aligned} \tag{9}$$

The matrix $\boldsymbol{M}$ is expressed as a nominal and perturbation term as well

$$\boldsymbol{M} = (\boldsymbol{M}_o + \boldsymbol{\delta}_M) \tag{10}$$

where

$$\begin{aligned}
\boldsymbol{M}_o &= \begin{bmatrix}\boldsymbol{M}_{o11} & \boldsymbol{M}_{o12}\\ \boldsymbol{M}_{o12} & \boldsymbol{M}_{o22}\end{bmatrix}\\
\boldsymbol{M}_{o11} &= L_1^2(\widetilde{M}_1 + \widetilde{M}_2) + L_2^2\widetilde{M}_2 + 2L_1L_2\widetilde{M}_2 cosq_2\\
\boldsymbol{M}_{o12} &= L_2^2\widetilde{M}_2 + L_1L_2\widetilde{M}_2 cosq_2\\
\boldsymbol{M}_{o22} &= L_2^2\widetilde{M}_2\\
\boldsymbol{\delta}_M &= \begin{bmatrix}\boldsymbol{\delta}_{M_{11}} & \boldsymbol{\delta}_{M_{12}}\\ \boldsymbol{\delta}_{M_{12}} & \boldsymbol{\delta}_{M_{22}}\end{bmatrix}\\
\boldsymbol{\delta}_{M_{11}} &= L_1^2(\delta_{m1} + \delta_{m2}) + L_2^2\delta_{m2} + 2L_1L_2\delta_{m2}cosq_2\\
\boldsymbol{\delta}_{M_{12}} &= L_2^2\delta_{m2} + L_1L_2\delta_{m2}cosq_2\\
\boldsymbol{\delta}_{M_{22}} &= L_2^2\delta_{m2}
\end{aligned} \tag{11}$$

The matrix inverse lemma is adopted to determine the inverse of matrix $\boldsymbol{M}$ as follows:

$$\begin{aligned}\boldsymbol{M}^{-1} &= \boldsymbol{G} + \Delta\boldsymbol{G}\\ \boldsymbol{G} &= \boldsymbol{M_o}^{-1}\\ \Delta\boldsymbol{G} &= -\boldsymbol{G}\left(\boldsymbol{G} + \boldsymbol{\delta_M}^{-1}\right)^{-1}\boldsymbol{G}\end{aligned} \tag{12}$$

Substituting (12) in (5) yields

$$\begin{aligned}\dot{\boldsymbol{z}}_1 &= \boldsymbol{z}_2\\ \dot{\boldsymbol{z}}_2 &= \boldsymbol{G}\boldsymbol{u}_s + \Delta\boldsymbol{G}\boldsymbol{u}_s + \boldsymbol{M}^{-1}\boldsymbol{\delta}_N\end{aligned} \tag{13}$$

Let $\boldsymbol{G}\boldsymbol{u}_s = \boldsymbol{V}$ with $\boldsymbol{V} = [\mathrm{v}_1\ \mathrm{v}_2]^{\mathbf{T}}$, then $\boldsymbol{u}_s = \boldsymbol{G}^{-1}\boldsymbol{V} = \boldsymbol{M}_o\boldsymbol{V}$ and (13) is described by

$$\begin{aligned}\dot{\boldsymbol{z}}_1 &= \boldsymbol{z}_2\\ \dot{\boldsymbol{z}}_2 &= \boldsymbol{V} + \Delta\boldsymbol{G}\boldsymbol{M}_o\boldsymbol{V} + \boldsymbol{M}^{-1}\boldsymbol{\delta}_N\end{aligned} \tag{14}$$

Let the sliding variable be defined as

$$\boldsymbol{s} = [s_1\ s_2]^T = \dot{\boldsymbol{e}} + \boldsymbol{\lambda}\boldsymbol{e} \tag{15}$$

where $\boldsymbol{\lambda} = diag(\lambda_1, \lambda_2)$, $\lambda_1, \lambda_2 \in \boldsymbol{\mathcal{R}}_+$ are positive constants, $\boldsymbol{e} = [e_1\ e_2]^T = \boldsymbol{z}_1 - \boldsymbol{r}$, and $\boldsymbol{r} = [r_1\ r_2]^T$ is the reference trajectory in the joint space.

Let $V_{s_1} = \frac{1}{2}s_1^2$ be a Lyapunov candidate for $\dot{s}_1$, then

$$\begin{aligned}\dot{V}_{s_1} &= s_1\dot{s}_1 = s_1[1\ 0](\ddot{\boldsymbol{e}} + \boldsymbol{\lambda}\dot{\boldsymbol{e}})\\ \Rightarrow s_1\dot{s}_1 &= s_1\left(\mathrm{v}_1 + [1\ 0]\Delta\boldsymbol{G}\boldsymbol{M}_o\boldsymbol{V} + \varphi_1(.)\right)\end{aligned} \tag{16}$$

where $\varphi_1(.) = [1 \quad 0]\boldsymbol{M}^{-1}\boldsymbol{\delta}_N - \ddot{r}_1 + \lambda_1\dot{q}_1 - \lambda_1\dot{r}_1$. Let $\mathrm{v}_1 = -k_1 sgn(s_1)$ with $k_1 \in \boldsymbol{\mathcal{R}}_+$ is a positive constant, then (16) is modified to (17).

$$s_1\dot{s}_1 \le -|s_1|(k_1 - [1 \quad 0]|\Delta\boldsymbol{G}||\boldsymbol{M}_o||\boldsymbol{V}| - |\varphi_1(.)|) \tag{17}$$

Choosing the gain k_1 as

$$k_1 \ge [1 \quad 0]|\Delta\boldsymbol{G}||\boldsymbol{M}_o||\boldsymbol{V}| + |\varphi_1(.)| + \eta_1 \tag{18}$$

where $|\varphi_1(.)| = [1 \quad 0]|\boldsymbol{M}^{-1}||\boldsymbol{\delta}_N| + |\ddot{r}_1| + \lambda_1|\dot{q}_1| + \lambda_1|\dot{r}_1|$, $\eta_1 \in \boldsymbol{\mathcal{R}}_+$ is a positive constant and the absolute values of $|\Delta\boldsymbol{G}|$, $|\boldsymbol{M}_o|$, $|\boldsymbol{V}|$, $|\boldsymbol{M}^{-1}|$, and $|\boldsymbol{\delta}_N|$ are to be understood component-wise. Then, (17) is rewritten as

$$s_1\dot{s}_1 \le -\eta_1|s_1| \tag{19}$$

By considering $V_{s_2} = \frac{1}{2}s_2^2$ as a Lyapunov candidate for $\dot{s}_2$ and setting $\mathrm{v}_2 = -k_2 sgn(s_2)$ with $k_2 \in \boldsymbol{\mathcal{R}}_+$ is a positive constant, and following the same reasoning as above, one obtains

$$k_2 \ge [0 \quad 1]|\Delta\boldsymbol{G}||\boldsymbol{M}_o||\boldsymbol{V}| + |\varphi_2(.)| + \eta_2 \tag{20}$$

where $|\varphi_2(.)| = [0 \quad 1]|\boldsymbol{M}^{-1}||\boldsymbol{\delta}_N| + |\ddot{r}_2| + \lambda_2|\dot{q}_2| + \lambda_2|\dot{r}_2|$, $\eta_2 \in \boldsymbol{\mathcal{R}}_+$ is a positive constant and

$$s_2\dot{s}_2 \le -\eta_2|s_2| \tag{21}$$

Equations (19) and (21) indicate that the reachability condition is satisfied, causing the error trajectories to be directed toward the sliding surfaces s_1 and s_2 in finite time and remain on them thereafter.

Combining (18) and (20) in the matrix form and noting that $|\boldsymbol{V}| \le \boldsymbol{K}$ and $\boldsymbol{K} = [k_1\ k_2]^T$, yields

$$\begin{aligned}&\boldsymbol{K} \ge |\Delta\boldsymbol{G}||\boldsymbol{M}_o|\boldsymbol{K} + |\widehat{\boldsymbol{\varphi}}(.)|\\ &\Rightarrow \boldsymbol{K}(\boldsymbol{I}_{2\mathbf{x}2} - |\Delta\boldsymbol{G}||\boldsymbol{M}_o|) \ge |\widehat{\boldsymbol{\varphi}}(.)|\\ &\Rightarrow \boldsymbol{K} \ge \boldsymbol{\xi}^{-1}|\widehat{\boldsymbol{\varphi}}(.)|\end{aligned} \tag{22}$$

where $\boldsymbol{\xi} = \boldsymbol{I}_{2\mathbf{x}2} - |\Delta\boldsymbol{G}||\boldsymbol{M}_o|$ and $|\widehat{\boldsymbol{\varphi}}(.)| = |\boldsymbol{M}^{-1}||\boldsymbol{\delta}_N| + \begin{bmatrix}\lambda_1(|\dot{q}_1| + |\dot{r}_1|) + |\ddot{r}_1| + \eta_1\\ \lambda_2(|\dot{q}_2| + |\dot{r}_2|) + |\ddot{r}_2| + \eta_2\end{bmatrix}$.

Remark 1: The only feasible solution for $\boldsymbol{K}$ in (22) is the positive one, indicating that every element of $\boldsymbol{K}$ is positive. This is evident from the assumptions underlying the design of $\boldsymbol{K}$.

Remark 2: For $\boldsymbol{K}$ to be a feasible solution, the matrix $\boldsymbol{\xi}^{-1}$ must have all positive elements, given that the elements of the vector $|\widehat{\boldsymbol{\varphi}}(.)|$ are positive. This requirement reduces to the condition that $\boldsymbol{\xi}$ be symmetric and positive definite, ensuring that each element in its inverse, $\boldsymbol{\xi}^{-1}$, is positive.

Finally, the control action is reformulated as

$$\boldsymbol{u} = \boldsymbol{M}_o\boldsymbol{V} + \boldsymbol{u}_0 \tag{23}$$

To determine the maximum uncertainty ranges, δ_{m1} and δ_{m2}, that the proposed method can accommodate, adhere to the following three steps:

1. Initialize $\hat{\delta}_{m1}$ and $\hat{\delta}_{m2}$ to small values
2. Determine the maximum value of $\Delta\boldsymbol{G}$ in terms of 2- norm using (12) across the ranges $\delta_{m1} = [-\hat{\delta}_{m1}, \hat{\delta}_{m1}]$, $\delta_{m2} = [-\hat{\delta}_{m2}, \hat{\delta}_{m2}]$, and $q_2 = [0, \pi]$. It is important to note that $\boldsymbol{M_o}$ is calculated with $q_2 = \pi/2$ to obtain the maximum permissible uncertainty values for δ_{m1} and δ_{m2}.
3. Check weather $\boldsymbol{\xi}$ is symmetric positive definite. If true, increase $\hat{\delta}_{m1}$ and $\hat{\delta}_{m2}$ by appropriate values and go to step 2; otherwise, consider the last $\Delta\boldsymbol{G}$, δ_{m1} and δ_{m2} values that satisfied the specified condition.

IV. Results and Discussion

The simulation of the presented two-link manipulator and the proposed component-wise SMC is implemented using MATLAB 2023a Simulink. The parameters used in the simulation are listed in Table I.

TABLE I. Parameters of the Manipulator and Proposed Controller Used in the Simulation

Parameter	Value
$\widetilde{M}_1$	10 kg
$\widetilde{M}_2$	1 kg
L_1, L_2	1 m
δ_{m1}	$0.27\widetilde{M}_1$
δ_{m2}	$0.27\widetilde{M}_2$
λ_1, λ_2	5
$\boldsymbol{G} = \boldsymbol{M_o}^{-1}$ (with $q_2 = \pi/2$)	$\begin{bmatrix} 12 & 1 \\ 1 & 1 \end{bmatrix}^{-1}$
$\Delta\boldsymbol{G}$	$\begin{bmatrix} -0.0159 & -0.0119 \\ -0.0119 & 0.4197 \end{bmatrix}$
$\lvert\boldsymbol{M}^{-1}\rvert = \lvert\boldsymbol{G} + \Delta\boldsymbol{G}\rvert$	$\begin{bmatrix} 0.0750 & 0.1028 \\ 0.1028 & 1.5106 \end{bmatrix}$
η_1, η_2	0.01

Note that the values for δ_{m1}, δ_{m2} and $\Delta\boldsymbol{G}$ in Table I are calculated using the three steps outlined above.

To verify the effectiveness of the proposed controller, two simulation scenarios are investigated. In the first scenario, the manipulator is required to track a circular trajectory, characterized by a center (x_{d_c}, y_{d_c}) and radius r_d, expressed in world coordinates (x, y) as [60]

$$\begin{aligned} x_d(t) &= x_{d_c} + r_d cos\psi_d \\ y_d(t) &= y_{d_c} + r_d sin\psi_d \\ \psi_d(t) &= 2\pi t/t_f - sin(2\pi t/t_f), \ \ 0 \le t \le t_f. \end{aligned} \tag{24}$$

In this scenario, the operational timeframe is initiated at $t = 0$ and terminates at $t = t_f$.

In the second scenario, the manipulator is tasked with following a figure-8 trajectory, characterized by a center (x_{d_c}, y_{d_c}), length l_d and width w_d, expressed in world coordinates (x, y) as

$$\begin{aligned} x_d(t) &= x_{d_c} + l_d cos\psi_d \\ y_d(t) &= y_{d_c} + w_d sin\psi_d cos\psi_d \\ \psi_d(t) &= 2\pi t/t_f - sin(2\pi t/t_f), \ \ 0 \le t \le t_f. \end{aligned} \tag{25}$$

It is important to note that $x_d(t)$ and $y_d(t)$ in (23) and (24) are converted to the desired values in the joint space using (2). In this scenario, the operation is initialized at time $t = 0$ and concludes at the terminal time $t = t_f$. The parameters for the two trajectories are selected as indicated in Table II.

In the two proposed scenarios, the discontinuous controllers are approximated to mitigate chattering by

$$\begin{aligned} v_1 &= -k_1 tanh(1000 s_1) \\ v_2 &= -k_2 tanh(1000 s_2). \end{aligned} \tag{26}$$

TABLE II. Parameters of the Desired Circular and Figure-8 Trajectory

Parameter	Value
x_{d_c},y_{d_c}	1 m
r_d	0.5 m
l_d	0.25 m
w_d	0.25 m
t_f	5 sec

Three cases are considered: 1) when there is no uncertainty in M_1 and M_2, 2) when there is +27% uncertainty in M_1 and M_2 , and 3) when there is -27% uncertainty in M_1 and M_2. In the first scenario, the initial position of the end effector is at $(x_0, y_0) = (1.3\ m, 1.2\ m)$. Fig. 2 (left) presents the desired and actual trajectory of the manipulator's end effector in Cartesian space when there is no uncertainty and 27% uncertainty in M_1 and M_2. The proposed controller shows superior tracking performance with a very small tracking error in each case. The tracking errors in joint space for each case are demonstrated in Fig. 3 (left). The control actions for every case are shown in Fig. 4 (left). Table III presents the performance indices used to demonstrate the superiority of the proposed controller over the two MIMO controllers introduced in [60] under nominal links' masses conditions. It is evident that the proposed controller achieves the lowest INU and the smallest peak values of control action, indicating its enhanced energy efficiency. Additionally, the proposed controller exhibits a smaller INE compared to the component-wise controller in [60]. While the vector control achieves a marginally smaller INE than the proposed controller, this comes at the cost of significantly higher energy consumption, thereby establishing the proposed controller as superior to both alternatives in terms of balancing accuracy and energy efficiency.

TABLE III. Control Signal Peak Values of the Proposed Controller and the Ones Proposed in [60]

Control method	INE	INU	Peak value of control action
Proposed component-wise controller	0.0616	43.595	58 Nm
Component-wise controller in [60]	0.0705	96.2046	92 Nm
Vector control in [60]	0.0605	4935.51	2000 Nm

The sliding manifolds for the three cases are presented in Fig. 5 (left). As can be noticed, once the trajectory enters the manifold, it remains on it, indicating that the chosen values of k_1 and k_2 are sufficient. The sliding manifold in the component-wise controller presented in [60] demonstrates a behavior where it intersects the zero line and subsequently reverts to it. This observation implies that the controller gains utilized in the design may be insufficient or improperly calibrated. Fig. 6 (left) depicts the controllers' gains for all cases. As demonstrated in Fig. 6 (left), the controller gains remain consistent across all cases once the trajectories enter the sliding manifolds. This behavior highlights the efficacy of the method used to determine the controllers' gains and underscores the robustness of the proposed controller in handling uncertainties related to the mass of the links.

In the second scenario, the initial position of the end effector is at $(x_0, y_0) = (1.3\,m, 1\,m)$. Fig. 2 (right) illustrates the desired and actual trajectories of the manipulator's end effector in Cartesian space under the following conditions: with no uncertainty and 27% uncertainty in M_1 and M_2. The proposed controller demonstrates excellent tracking performance, exhibiting minimal tracking error in all cases. The tracking errors in joint space for each case are depicted in Fig. 3 (right). The control signals for all cases are shown in Fig. 4 right). The sliding manifolds for the three cases are presented in Fig. 5 (right). As can be noticed, once the trajectory enters the manifold, it remains on it, indicating that the chosen values of k_1 and k_2 are sufficient. Fig. 6 (right) depicts the controllers' gains for all cases.

The controller exhibits robust performance in tracking both circular and figure-8 trajectories, demonstrating minimal tracking error and control effort. Notably, the figure-8 trajectory, characterized by its complex curvature, posed a more demanding challenge. Nevertheless, the controller maintained its effectiveness, even in the presence of mass uncertainties. These results highlight the controller's ability to handle diverse trajectory profiles. While the computational complexity of the proposed controller may be higher compared to the methods presented in [60], it offers significant advantages. Notably, the proposed controller guarantees robust stability and performance under link masses uncertainties. Furthermore, its computational burden can be significantly reduced by pre-computing the inverse of the matrices involved in the control gains.

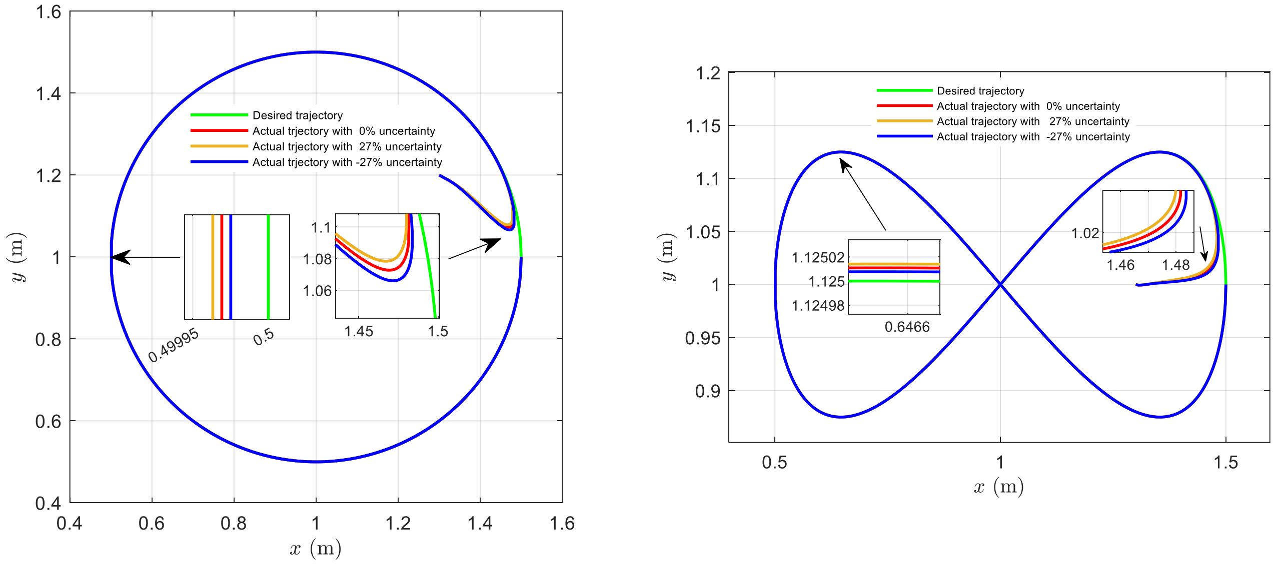

Fig. 2. Desired and actual trajectories of the manipulator's end effector in Cartesian space when there is no uncertainty and 27% uncertainty in M_1 and M_2. Circular trajectory (left) and figure-8 trajectory (right)

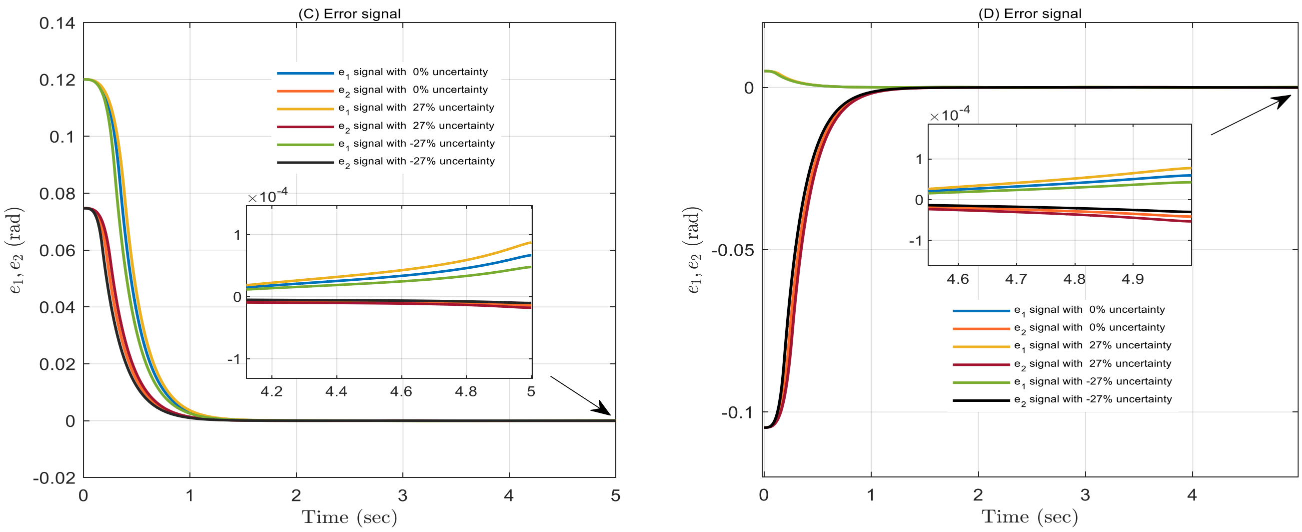

Fig. 3. The tracking error trajectories in joint space with and without link masses uncertainties. Circular trajectory (left) and figure-8 trajectory (right)

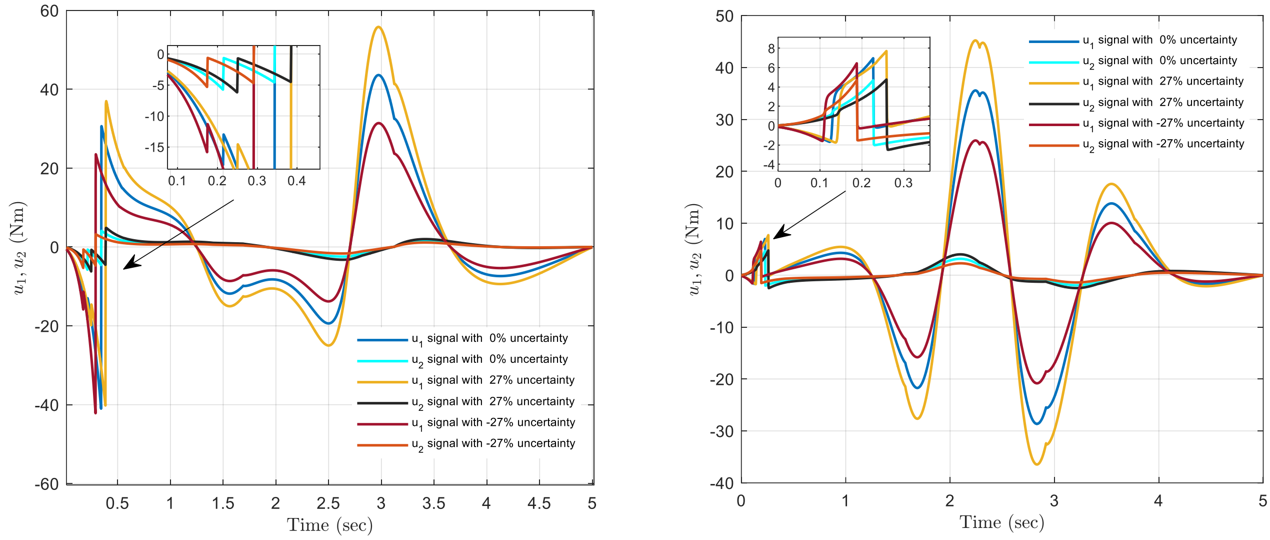

Fig. 4. The control actions when there is 0% and 27% uncertainty in links' masses. Circular trajectory (left) and figure-8 trajectory (right)

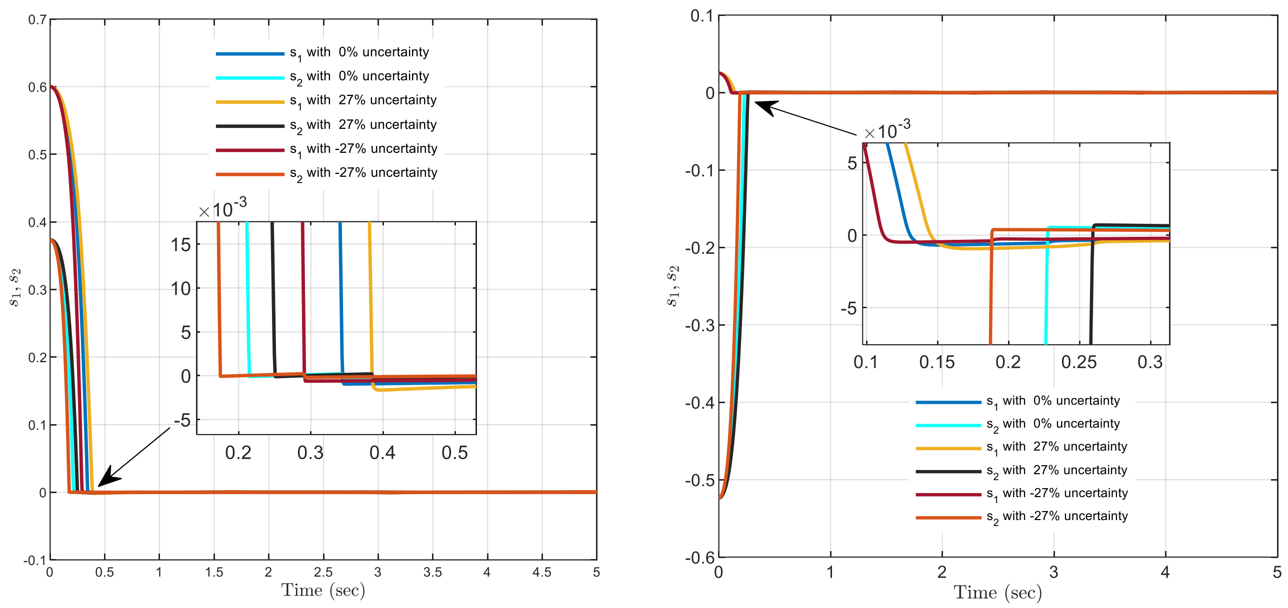

Fig. 5. The sliding manifolds for the three cases. Circular trajectory (left) and figure-8 trajectory (right)

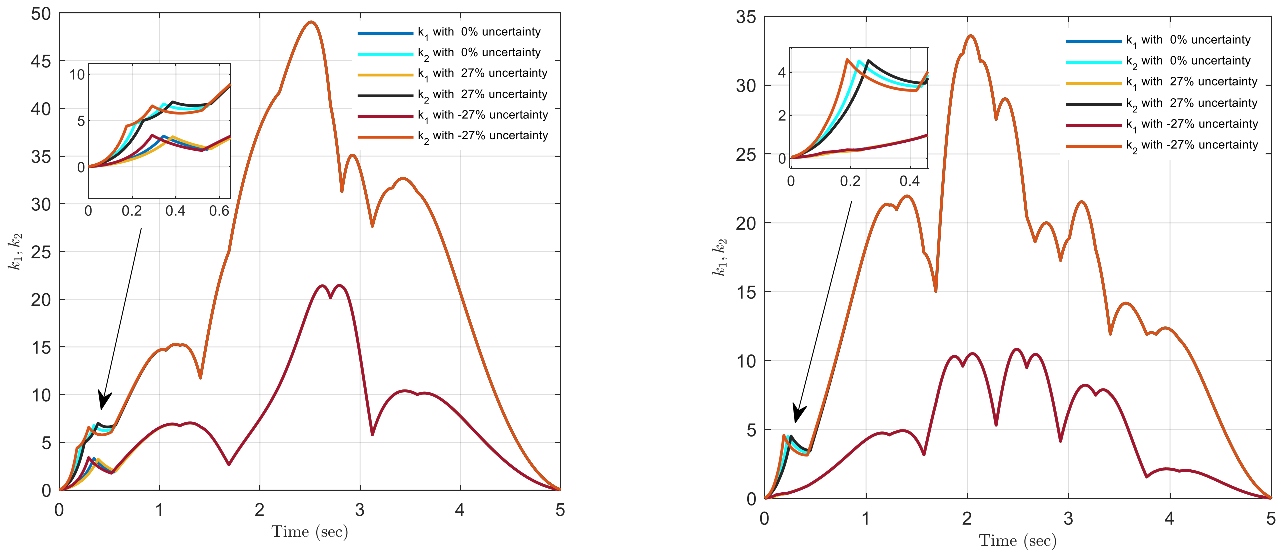

Fig. 6. The controllers' gains under 0% and 0% link masses uncertainties. Circular trajectory (left) and figure-8 trajectory (right)

V. Conclusion

A component-wise SMC controller was developed for a two-link manipulator. The uncertainty conditions that led to feasible controller gains are thoroughly analyzed. The proposed methodology exhibited robustness to mass uncertainties of up to 27% in the manipulator's links, indicating its suitability for controlling a two-link manipulator operating within this uncertainty bound. The efficacy of the proposed controller was assessed using two distinct trajectories, circular and figure-8, under both nominal conditions and with 27% mass uncertainty in the system's links. Simulation outcomes demonstrated enhanced trajectory tracking performance with comparatively modest control inputs when contrasted with other component-wise/MIMO sliding mode control methodologies, despite the fact that these methods neglected the consideration of link masses uncertainties in their analyses. Notably, the computational complexity of the proposed controller is relatively low due to the fact that the inverse of the matrices in the gain equation can be pre-computed offline. Future work will focus on the experimental validation of the proposed controller on a real two-link manipulator and its extension to more complex serial and parallel manipulators. Additionally, A promising area for future research is to evaluate the controller's performance in the presence of external disturbances and high-frequency noise.

References

[1] B. Zhang, Y. Xie, J. Zhou, K. Wang, and Z. Zhang, "State-of-the-art robotic grippers, grasping and control strategies, as well as their applications in agricultural robots: A review," *Computers and Electronics in Agriculture*, vol. 177, p. 105694, Oct. 2020, doi: 10.1016/j.compag.2020.105694.

[2] Y. H. Alnema, M. Almaged, and M. N. Noaman, "Driverless Model Cars: a Review and Analysis of Autonomous Vehicle Literature on Technology and Application," *International Review of Automatic Control (IREACO)*, vol. 13, no. 2, p. 84, Mar. 2020, doi: 10.15866/ireaco.v13i2.18659.

[3] A. Sathish Kumar *et al*., "An intelligent fuzzy-particle swarm optimization supervisory-based control of robot manipulator for industrial welding applications," *Scientific Reports*, vol. 13, no. 1, May 2023, doi: 10.1038/s41598-023-35189-2.

[4] L. Zongxing, L. Wanxin, and Z. Liping, "Research development of soft manipulator: A review," *Advances in Mechanical Engineering*, vol. 12, no. 8, Aug. 2014, doi: 10.1177/1687814020950094.

[5] Z. Liu, K. Peng, L. Han, and S. Guan, "Modeling and Control of Robotic Manipulators Based on Artificial Neural Networks: A Review," *Iranian Journal of Science and Technology, Transactions of Mechanical Engineering*, vol. 47, no. 4, pp. 1307–1347, Jan. 2023, doi: 10.1007/s40997-023-00596-3.

[6] N. Tan, C. Li, P. Yu, and F. Ni, "Two model-free schemes for solving kinematic tracking control of redundant manipulators using CMAC networks," *Applied Soft Computing*, vol. 126, p. 109267, Sep. 2022, doi: 10.1016/j.asoc.2022.109267.

[7] J. Perez and M. S. L. de la Fuente, "Trajectory Tracking Error Using Fractional Order PID Control Law for Two-Link Robot Manipulator via Fractional Adaptive Neural Networks," *Robotics - Legal, Ethical and Socioeconomic Impacts*, Dec. 2017, doi: 10.5772/intechopen.70020.

[8] Q. V. Doan, A. T. Vo, T. D. Le, H.-J. Kang, and N. H. A. Nguyen, "A Novel Fast Terminal Sliding Mode Tracking Control Methodology for Robot Manipulators," *Applied Sciences*, vol. 10, no. 9, p. 3010, Apr. 2020, doi: 10.3390/app10093010.

[9] S. Jia and J. Shan, "Finite-Time Trajectory Tracking Control of Space Manipulator Under Actuator Saturation," *IEEE Transactions on Industrial Electronics*, vol. 67, no. 3, pp. 2086–2096, Mar. 2020, doi: 10.1109/tie.2019.2902789.

[10] S. Tian and T. Zhao, "Self-organizing interval type-2 function-link fuzzy neural network control for uncertain manipulators under saturation: A predefined-time sliding-mode approach," *Applied Soft Computing*, vol. 165, p. 112064, Nov. 2024, doi: 10.1016/j.asoc.2024.112064.

[11] S. I. Abdelmaksoud, M. H. Al-Mola, G. E. M. Abro, and V. S. Asirvadam, "In-Depth Review of Advanced Control Strategies and Cutting-Edge Trends in Robot Manipulators: Analyzing the Latest Developments and Techniques," *IEEE Access*, vol. 12, pp. 47672–47701, 2024, doi: 10.1109/access.2024.3383782.

[12] A. Billard and D. Kragic, "Trends and challenges in robot manipulation," *Science*, vol. 364, no. 6446, Jun. 2019, doi: 10.1126/science.aat8414.

[13] T. Q. Ngo, T. H. Tran, T. T. H. Le, and B. M. Lam, "An Application of Modified T2FHC Algorithm in Two-Link Robot Controller," *Journal of Robotics and Control (JRC)*, vol. 4, no. 4, pp. 509–520, Aug. 2023, doi: 10.18196/jrc.v4i4.18943.

[14] F. Wang *et al*., "Sliding Mode Robust Active Disturbance Rejection Control for Single-Link Flexible Arm with Large Payload Variations," *Electronics*, vol. 10, no. 23, p. 2995, Dec. 2021, doi: 10.3390/electronics10232995.

[15] A. Ollero, M. Tognon, A. Suarez, D. Lee, and A. Franchi, "Past, Present, and Future of Aerial Robotic Manipulators," *IEEE Transactions on Robotics*, vol. 38, no. 1, pp. 626–645, Feb. 2022, doi: 10.1109/tro.2021.3084395.

[16] J. Liu, L. Wu, C. Wu, W. Luo, and L. G. Franquelo, "Event-triggering dissipative control of switched stochastic systems via sliding mode," *Automatica*, vol. 103, pp. 261–273, May 2019, doi: 10.1016/j.automatica.2019.01.029.

[17] J. Kumar, V. Kumar, and K. P. S. Rana, "Fractional-order self-tuned fuzzy PID controller for three-link robotic manipulator system," *Neural Computing and Applications*, vol. 32, no. 11, pp. 7235–7257, May 2019, doi: 10.1007/s00521-019-04215-8.

[18] E. Kelekci and S. Kizir, "Trajectory and vibration control of a flexible joint manipulator using interval type-2 fuzzy logic," *ISA Transactions*, vol. 94, pp. 218–233, Nov. 2019, doi: 10.1016/j.isatra.2019.04.001.

[19] X. Guo, H. Zhang, J. Sun, and Y. Zhou, "Fixed-Time Fuzzy Adaptive Control of Manipulator Systems Under Multiple Constraints: A Modified Dynamic Surface Control Approach," *IEEE Transactions on Systems, Man, and Cybernetics: Systems*, vol. 53, no. 4, pp. 2522–2532, Apr. 2023, doi: 10.1109/tsmc.2022.3212988.

[20] I. K. Mohammed and M. N. Noaman, "Optimal Control Approach for Robot System Using LQG Technique," *Journal Européen des Systèmes Automatisés*, vol. 55, no. 5, pp. 671–677, Nov. 2022, doi: 10.18280/jesa.550513.

[21] M. N. Alghanim, M. Qasim, K. P. Valavanis, M. J. Rutherford, and M. Stefanovic, "Passivity-Based Adaptive Controller for Dynamic Self-Leveling of a Custom-Built Landing Platform on Top of a UGV," *2020 28th Mediterranean Conference on Control and Automation (MED)*, pp. 458–464, Sep. 2020, doi: 10.1109/med48518.2020.9182807.

[22] B. Rahmani and M. Belkheiri, "Adaptive neural network output feedback control for flexible multi-link robotic manipulators," *International Journal of Control*, vol. 92, no. 10, pp. 2324–2338, Feb. 2018, doi: 10.1080/00207179.2018.1436774.

[23] O. Tutsoy and D. E. Barkana, "Model free adaptive control of the under-actuated robot manipulator with the chaotic dynamics," *ISA Transactions*, vol. 118, pp. 106–115, Dec. 2021, doi: 10.1016/j.isatra.2021.02.006.

[24] M. N. Alghanim, M. Qasim, K. P. Valavanis, M. J. Rutherford, and M. Stefanovic, "Comparison of Controller Performance for UGV-Landing Platform Self-Leveling," *2020 28th Mediterranean Conference on Control and Automation (MED)*, pp. 471–478, Sep. 2020, doi: 10.1109/med48518.2020.9182837.

[25] J. Wu, Z. Jin, A. Liu, and L. Yu, "Vision-based neural predictive tracking control for multi-manipulator systems with parametric uncertainty," *ISA Transactions*, vol. 110, pp. 247–257, Apr. 2021, doi: 10.1016/j.isatra.2020.10.057.

[26] W. Xu, P. Yan, F. Wang, H. Yuan, and B. Liang, "Vision-based simultaneous measurement of manipulator configuration and target pose for an intelligent cable-driven robot," *Mechanical Systems and Signal Processing*, vol. 165, p. 108347, Feb. 2022, doi: 10.1016/j.ymssp.2021.108347.

[27] M. Noaman, M. Qasim, and O. Ismael, “Landmarks exploration algorithm for mobile robot indoor localization using VISION sensor,” *Journal of Engineering Science and Technology*, vol. 16, no. 4, pp. 3165–3184, 2021.

[28] K. Jayaswal, D. K. Palwalia, and S. Kumar, “Performance investigation of PID controller in trajectory control of two-link robotic manipulator in medical robots,” *Journal of Interdisciplinary Mathematics*, vol. 24, no. 2, pp. 467–478, Feb. 2021, doi: 10.1080/09720502.2021.1893444.

[29] P. Chotikunnan and R. Chotikunnan, “Dual Design PID Controller for Robotic Manipulator Application,” *Journal of Robotics and Control (JRC)*, vol. 4, no. 1, pp. 23–34, Feb. 2023, doi: 10.18196/jrc.v4i1.16990.

[30] M. J. Mohamed, B. K. Oleiwi, L. H. Abood, A. T. Azar, and I. A. Hameed, “Neural fractional order PID controllers design for 2-link rigid robot manipulator,” *Fractal and Fractional*, vol. 7, no. 9, p. 693, 2023.

[31] S. Luo, M. Cheng, R. Ding, F. Wang, B. Xu, and B. Chen, “Human–Robot Shared Control Based on Locally Weighted Intent Prediction for a Teleoperated Hydraulic Manipulator System,” *IEEE/ASME Transactions on Mechatronics*, vol. 27, no. 6, pp. 4462–4474, Dec. 2022, doi: 10.1109/tmech.2022.3157852.

[32] D. Rakita, B. Mutlu, M. Gleicher, and L. M. Hiatt, “Shared control–based bimanual robot manipulation,” *Science Robotics*, vol. 4, no. 30, May 2019, doi: 10.1126/scirobotics.aaw0955.

[33] M. Qasim and O. Y. Ismael, “Shared Control of a Robot Arm Using BCI and Computer Vision,” Journal Européen des Systèmes Automatisés, vol. 55, no. 1, pp. 139–146, Feb. 2022, doi: 10.18280/jesa.550115.

[34] A. Liu, H. Zhao, T. Song, Z. Liu, H. Wang, and D. Sun, “Adaptive control of manipulator based on neural network,” *Neural Computing and Applications*, vol. 33, no. 9, pp. 4077–4085, Nov. 2020, doi: 10.1007/s00521-020-05515-0.

[35] F. Luan, J. Na, Y. Huang, and G. Gao, “Adaptive neural network control for robotic manipulators with guaranteed finite-time convergence,” *Neurocomputing*, vol. 337, pp. 153–164, Apr. 2019, doi: 10.1016/j.neucom.2019.01.063.

[36] Q. Zhou, S. Zhao, H. Li, R. Lu, and C. Wu, “Adaptive Neural Network Tracking Control for Robotic Manipulators With Dead Zone,” *IEEE Transactions on Neural Networks and Learning Systems*, vol. 30, no. 12, pp. 3611–3620, Dec. 2019, doi: 10.1109/tnnls.2018.2869375.

[37] L. Dai, Y. Yu, D.-H. Zhai, T. Huang, and Y. Xia, “Robust Model Predictive Tracking Control for Robot Manipulators With Disturbances,” *IEEE Transactions on Industrial Electronics*, vol. 68, no. 5, pp. 4288–4297, May 2021, doi: 10.1109/tie.2020.2984986.

[38] M. Krämer, C. Rösmann, F. Hoffmann, and T. Bertram, “Model predictive control of a collaborative manipulator considering dynamic obstacles,” Optimal Control Applications and Methods, vol. 41, no. 4, pp. 1211–1232, Apr. 2020, doi: 10.1002/oca.2599.

[39] O. Y. Ismael, M. N. Noaman, and I. K. Abdullah, “Fick’s Law Algorithm Based-Nonlinear Model Predictive Control of Twin Rotor MIMO System,” *Journal of Robotics and Control (JRC)*, vol. 5, no. 3, pp. 694–705, 2024, doi: 10.18196/jrc.v5i3.21725.

[40] M. Elsisi, K. Mahmoud, M. Lehtonen, and M. M. F. Darwish, “Effective Nonlinear Model Predictive Control Scheme Tuned by Improved NN for Robotic Manipulators,” *IEEE Access*, vol. 9, pp. 64278–64290, 2021, doi: 10.1109/access.2021.3075581.

[41] M. S. Qasim, A. B. Ayoub, and A. I. Abdulla, “NMPC Based-Trajectory Tracking and Obstacle Avoidance for Mobile Robots,” *International Journal of Robotics and Control Systems*, vol. 4, no. 4, pp. 2026–2040, Nov. 2024, doi: 10.31763/ijrcs.v4i4.1605.

[42] M. J. Mahmoodabadi and N. Nejadkourki, “Trajectory Tracking of a Flexible Robot Manipulator by a New Optimized Fuzzy Adaptive Sliding Mode-Based Feedback Linearization Controller,” *Journal of Robotics*, vol. 2020, pp. 1–12, Jul. 2020, doi: 10.1155/2020/8813217.

[43] M. Bagheri, P. Naseradinmousavi, and M. Krstić, “Feedback linearization based predictor for time delay control of a high-DOF robot manipulator,” *Automatica*, vol. 108, p. 108485, Oct. 2019, doi: 10.1016/j.automatica.2019.06.037.

[44] O. Y. Ismael, M. Qasim, M. N. Noaman, and A. Kurniawan, “Salp Swarm Algorithm-Based Nonlinear Robust Control of Magnetic Levitation System Using Feedback Linearization Approach,” *Proceedings of the 3rd International Conference on Electronics, Communications and Control Engineering*, pp. 58–64, Apr. 2020, doi: 10.1145/3396730.3396734.

[45] S. J. Gambhire, D. R. Kishore, P. S. Londhe, and S. N. Pawar, “Review of sliding mode based control techniques for control system applications,” *International Journal of Dynamics and Control*, vol. 9, no. 1, pp. 363–378, May 2020, doi: 10.1007/s40435-020-00638-7.

[46] J. Hu, X. Zhang, D. Zhang, Y. Chen, H. Ni, and H. Liang, “Finite-time adaptive super-twisting sliding mode control for autonomous robotic manipulators with actuator faults,” *ISA Transactions*, vol. 144, pp. 342–351, Jan. 2024, doi: 10.1016/j.isatra.2023.10.028.

[47] O. Y. Ismael, M. Qasim, and M. N. Noaman, “Equilibrium Optimizer-Based Robust Sliding Mode Control of Magnetic Levitation System,” *Journal Européen des Systèmes Automatisés*, vol. 54, no. 1, pp. 131–138, Feb. 2021, doi: 10.18280/jesa.540115.

[48] T. N. Truong, A. T. Vo, and H.-J. Kang, “A Backstepping Global Fast Terminal Sliding Mode Control for Trajectory Tracking Control of Industrial Robotic Manipulators,” *IEEE Access*, vol. 9, pp. 31921–31931, 2021, doi: 10.1109/access.2021.3060115.

[49] A. Q. Al-Dujaili, A. Falah, A. J. Humaidi, D. A. Pereira, and I. K. Ibraheem, “Optimal super-twisting sliding mode control design of robot manipulator: Design and comparison study,” *International Journal of Advanced Robotic Systems*, vol. 17, no. 6, Nov. 2020, doi: 10.1177/1729881420981524.

[50] Y. Guo and B.-L. Ma, “Global sliding mode with fractional operators and application to control robot manipulators,” *International Journal of Control*, vol. 92, no. 7, pp. 1497–1510, Nov. 2017, doi: 10.1080/00207179.2017.1398417.

[51] A. T. Vo and H.-J. Kang, “A Novel Fault-Tolerant Control Method for Robot Manipulators Based on Non-Singular Fast Terminal Sliding Mode Control and Disturbance Observer,” *IEEE Access*, vol. 8, pp. 109388–109400, 2020, doi: 10.1109/access.2020.3001391.

[52] J. Liu, L. Wu, C. Wu, W. Luo, and L. G. Franquelo, “Event-triggering dissipative control of switched stochastic systems via sliding mode,” *Automatica*, vol. 103, pp. 261–273, May 2019, doi: 10.1016/j.automatica.2019.01.029.

[53] S. Mobayen, O. Mofid, S. U. Din, and A. Bartoszewicz, “Finite-Time Tracking Controller Design of Perturbed Robotic Manipulator Based on Adaptive Second-Order Sliding Mode Control Method,” *IEEE Access*, vol. 9, pp. 71159–71169, 2021, doi: 10.1109/access.2021.3078760.

[54] T. N. Truong, A. T. Vo, and H.-J. Kang, “Neural network-based sliding mode controllers applied to robot manipulators: A review,” *Neurocomputing*, vol. 562, p. 126896, Dec. 2023, doi: 10.1016/j.neucom.2023.126896.

[55] E. A. Alandoli and T. S. Lee, “A Critical Review of Control Techniques for Flexible and Rigid Link Manipulators,” *Robotica*, vol. 38, no. 12, pp. 2239–2265, May 2020, doi: 10.1017/s0263574720000223.

[56] S. Jung, “Improvement of Tracking Control of a Sliding Mode Controller for Robot Manipulators by a Neural Network,” *International Journal of Control, Automation and Systems*, vol. 16, no. 2, pp. 937–943, Apr. 2018, doi: 10.1007/s12555-017-0186-z.

[57] A. S. Poznyak, A. V. Nazin, and H. Alazki, “Integral Sliding Mode Convex Optimization in Uncertain Lagrangian Systems Driven by PMDC Motors: Averaged Subgradient Approach,” *IEEE Transactions on Automatic Control*, vol. 66, no. 9, pp. 4267–4273, Sep. 2021, doi: 10.1109/tac.2020.3032088.

[58] B. Özyer “Adaptive fast sliding neural control for robot manipulator,” *Turkish Journal of Electrical Engineering and Computer Sciences*, vol. 28, no. 6, Nov. 2020, doi: 10.3906/elk-2001-129.

[59] O. Eray and S. Tokat, “The design of a fractional-order sliding mode controller with a time-varying sliding surface,” *Transactions of the Institute of Measurement and Control*, vol. 42, no. 16, pp. 3196–3215, Aug. 2020, doi: 10.1177/0142331220944626.

[60] V. Utkin, J. Guldner, and J. Shi. *Sliding Mode Control in Electro-Mechanical Systems*. CRC Press, 2017, doi: 10.1201/9781420065619.